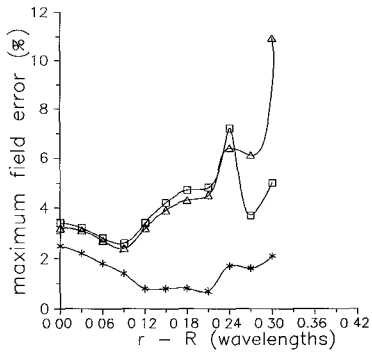

Fig. 3. Solution error versus r-R which is the distance from the metallic sphere scatterer. The radius of the metallic sphere is $R = 0.3\lambda$, and $D = 0.3\lambda$. The stars show the error using the complete form of the second order vector ABC and enforcing normal field continuity on the ABS. The triangles show the error when normal continuity has not been enforced on the ABS, and the squares show the error when in addition to the absence of the normal continuity enforcement, the surface divergence term was absent from the functional.

over the volume modeled, expressed as a percentage of $|\mathbf{H}^s_{\text{analytical}}|$ at the point where the largest value of e occurs. Fine meshes were used so that the discretization errors were reduced to a minimum.

Fig. 3 show the errors for the cases 1), 2), and 3), when $D = 0.3\lambda$. It is clear that in case a) the results are far more accurate than those in cases 2) and 3). In fact, cases 2) and 3) appear to give about the same accuracy in the computed field.

IV. Conclusion

Due to the presence of the surface divergence term, the proper implementation of the second order absorbing boundary condition requires that the two extra conditions be explicitly enforced:

1) On the ABS, normal continuity has to be imposed between the quadrilaterals the ABS is divided into;
2) for the magnetic field case, where the ABS meets an electric wall, the component of magnetic field normal to the wall must be set to zero explicitly; for the electric field case, where the ABS meets a magnetic wall, the component of electric field normal to the wall must be set to zero explicitly.

Numerical results confirm the theory. If the second order ABC is to be used, then the two above conditions are necessary. If they are not imposed, then the error in the near field increases by a factor of at least two. In addition, if these two conditions are not imposed, the numerical results showed that the surface divergence term might as well be dropped out from the formulation.

Acknowledgment

The authors are grateful to Prof. T. D. Tsiboukis for his help and kind support, and to the Electrical Engineering Department (Telecommunications Division) of Aristotle University of Thessaloniki for using its facilities.

References

[1] A. F. Peterson, "Absorbing boundary conditions for the vector wave equation," *Microwave and Optical Technol. Lett.*, vol. 1, no. 2, pp. 62–64, Apr. 1988.

[2] J. M. Jin and J. L. Volakis, "A finite element-boundary integral formulation for scattering by three-dimensional cavity-backed apertures," *IEEE Trans. Antennas Propagat.*, 39, no. 1, pp. 97–104, Jan. 1991.

[3] J. P. Webb and V. N. Kanellopoulos, "Absorbing boundary conditions for the finite element solution of the vector wave equation," *Microwave and Optical Technol. Lett.*, vol. 2, no. 10, pp. 370–372, Oct. 1989.

[4] ——, "A numerical study of vector absorbing boundary conditions for the finite-element solution of Maxwell's equations," *IEEE Microwave and Guided Wave Lett.*, vol. 1, no. 11, pp. 325–327, Nov. 1991.

[5] ——, "3-D finite element analysis of a metallic sphere scatterer: Comparison of first and second order vector absorbing boundary conditions," *Journal de Physique III France 3*, pp. 563–572, Mar. 1993.

[6] ——, "Modeling the electromagnetic field in lossy dielectrics using finite elements and vector absorbing boundary conditions," *IEEE Trans. Microwave Theory and Tech.*, vol. 43, no. 4, pp. 823–827, Apr. 1995.

[7] A. Chatterjee, J. M. Jin, and J. L. Volakis, "Edge-Based Finite Elements and Vector ABC's Applied to 3-D Scattering," *IEEE Trans. Antennas Propagat.*, 41, no. 2, pp. 221–226, Feb. 1993.

[8] A. Chatterjee and J. L. Volakis, "Conformal absorbing boundary conditions for the vector wave equation," *Microwave and Opt. Technol. Lett.*, vol. 6, no. 16, pp. 886–889, Dec. 1993.

[9] V. N. Kanellopoulos, "Finite elements and vector absorbing boundary conditions in 3-D," Ph.D. Thesis, McGill Univ., Montréal, Canada, 1991.

[10] J. P. Webb, "Edge Elements and what they can do for you," *IEEE Trans. Magnetics*, 29, no. 2, pp. 1460–1465, Mar. 1993.

[11] C. Crowley, P. P. Silvester, and H. Hurwitz, Jr., "Covariant projection elements for 3-D vector field problems," *IEEE Trans. Magnetics*, 24, no. 1, pp. 397–400, Jan. 1988.

[12] J. Van Bladel, *Electromagnetic Fields*. New York: McGraw-Hill, 1964.

[13] R. F. Harrington, *Time-Harmonic Electromagnetic. Fields* New York: McGraw-Hill, 1961.

Coupling of the PISCES Device Modeler to a 3-D Maxwell FDTD Solver

Vincent A. Thomas, Michael E. Jones, and Rodney J. Mason

***Abstract*—We show how PISCES-like semiconductor models can be joined non-invasively to finite difference time domain models for the calculation of coupled external electromagnetics. The method involves "tricking" the standard current boundary condition for the device model into accepting an effective parallel external capacitance. For nearly steady state device conditions we show the results for a transmission line-coupled PISCES diode to agree well with those for an ideal diode.**

I. Introduction

The FDTD method advances Maxwell's equations in time on a finite difference mesh [1]. It is being used increasingly to analyze microwave circuits. Sui *et al.* [2] have shown how it might be extended to systems including active elements. Also, two of us recently demonstrated a technique [3] for robustly coupling FDTD to SPICE [4] circuit simulators for subgrid scale modeling. The present note extends this technique to provide coupling noninvasively of FDTD to the PISCES [5] device modeler. We demonstrate this procedure with application to a diode fixed to the end of a transmission line.

Manuscript received September 29, 1994; revised February 15, 1995. This work was supported in part by a cooperative research agreement between Cray Research, Inc. and the Los Alamos National Laboratory.

The authors are with the Los Alamos National Laboratory, Los Alamos, NM 87545 USA.

IEEE Log Number 9413409.

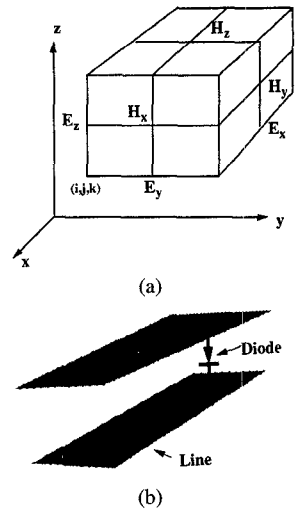

Fig. 1. (a) The mesh used for FDTD. (b) Diode at end of a microstrip line.

II. Approach and Results

The conventional FDTD approach solves the Maxwell equations

$$\epsilon\frac{\partial \mathbf{E}}{\partial t} + \mathbf{J}(\mathbf{E}) = \nabla \times \mathbf{H}. \tag{1a}$$

$$\frac{\partial \mathbf{H}}{\partial t} = -\mu\nabla \times \mathbf{E} \tag{1b}$$

with centered time and space differencing [5] on the Yee mesh [6], Fig. 1(a). The local current density $\mathbf{J}$ is given as a non-linear function of the electric field $\mathbf{E}$.

Consider the metal strip lines modeled with this mesh and feeding the diode of Fig. 1(b). In the free space regions $\mathbf{J} = 0$. Within the metal strips $\mathbf{J} = \sigma\mathbf{E}$, where σ is the electrical conductivity. To advance $\mathbf{E}$ from time level (m) to level $(m+1)$ one traditionally uses a centering [2] $\mathbf{J}^{(m+1/2)} = \sigma(\mathbf{E}^{(m+1)} + \mathbf{E}^{m})/2$. Then, with $\nabla \times \mathbf{H}^{(m+1/2)}$ known from a leap frog integration of (1b), the new E-field from the time advance of (1a) is

$$\mathbf{E}^{(m+1)} = \mathbf{E}^{(m)}\frac{\left[1-\frac{1}{2}\alpha\Delta t\right]}{\left[1+\frac{1}{2}\alpha\Delta t\right]} + \frac{\nabla \times \mathbf{H}^{(m+1/2)}\Delta t}{\epsilon\left[1+\frac{1}{2}\alpha\Delta t\right]} \tag{2}$$

with $\alpha = \sigma/\epsilon$. In the metal where the conductivity is large $\alpha \to \infty$, and $\mathbf{E}^{(m+1)} \to -\mathbf{E}^{(m)} + \nabla \times \mathbf{H}^{(m+1/2)}/\sigma$. The E-field is conserved, but it will evidence Nyquist oscillations from one time step to the next. On the average at half times $\mathbf{E}^{(m+1/2)} = \nabla \times \mathbf{H}^{(m+1/2)}/\sigma$.

Alternatively, the unwanted oscillations can be eliminated by treating (1b) as an ordinary differential equation in time with the right-hand side constant [7]. This corresponds to the approach taken in [8] for spatial differencing. Within the resistive metal this gives

$$\mathbf{E}^{(m+1)} = \mathbf{E}^{(m)}e^{-\alpha\Delta t} + \frac{\nabla \times \mathbf{H}^{(m+1/2)}}{\sigma}[1-e^{-\alpha\Delta t}]. \tag{3}$$

For large conductivities (3) gives $\mathbf{E}^{(m+1)} \to \nabla \times \mathbf{H}^{(m+1/2)}/\sigma$. In general, we have found this procedure to be more accurate and stable than (2).

For lumped elements connecting the transmission lines on various parts of the mesh, as in the case of the diode in Fig. 1(b), one can generalize this by transforming (1a) to

$$C\frac{dV}{dt} + I(V) = I_d \tag{4}$$

where for one possible orientation on the mesh the drive voltage V is defined as $\Delta y E$ with Δy running across the element, $C = \epsilon A/\Delta y$ is an effective capacitance in its neighborhood with $A = \Delta x \Delta z$ the local area of cell surfaces on the mesh, and Δy is the distance between nodes occupied by the element. The total current flowing though the element is $I(V) = AJ$, and $I_d = \mu A \nabla \times \mathbf{H}$ is an effective drive current (established by the local $\mathbf{H}$ gradients) feeding both the element and its local capacitance.

For simple elements such as the resistor, capacitor, inductor, and the ideal diode (4) can be integrated analytically and directly over Δt, as for (3). For a more complex collection of lumped elements across the mesh nodes [3] showed that the left-hand side of (4), i.e., voltage across both the lumped elements and the parallel mesh capacitance, can be efficiently integrated with the SPICE [4] package.

In some instances, however, the circuit coupled behavior of lumped elements is insufficiently characterized for SPICE, so that a device model is needed to furnish $I(V)$. Typically then, a PISCES [5]-like model would be used. We will now show how PISCES can be used to model a real diode between transmission lines on the mesh, as shown in Fig. 1(b). PISCES will readily provide a history for $V = V(I)$ across a solitary device. However, no option exists in the standard code to calculate voltage across a device in parallel with a capacitor. For this "mixed mode" situation several approaches at first seem plausible: 1) The matrix elements inside the Newtonian solver in PISCES can be augmented to include the capacitor's effects. Unfortunately for most users, this implies an unlikely access to the commercial source code. 2) With numerical derivatives calculated from PISCES one might form $I(V^{(m+1)}) = I(V^{(m)}) + \frac{dI^{(m)}}{dV}[V^{(m+1)} - V^{(m)}]$, and solve (4) with this for the new $V^{(m+1)}$. We found this to unstable at the time steps usually controlling FDTD. 3) One can "trick" standard PISCES into including the capacitor properly. This last approach is simple and successful.

Standard PISCES permits the use of a capacitor C and a resistor R in a "parallel RC combination" in series with a device under an applied voltage source V_{app} across the full system, and can derive a voltage V across the device carrying a current I. It employs the general boundary condition

$$\frac{(V_{app}-V)}{R} + C\frac{d(V_{app}-V)}{dt} = I_n + I_p + I_{disp} = I(V). \tag{5}$$

Here $I_{n,p}$ refers to current in the electrons and holes, and I_{disp} is the internal displacement current calculated in the device. The successful trick is to change V_{app} abruptly at the start of each new FDTD time step. Then PISCES neglects the dV_{app}/dt term in (5) (because it is infinite). One can then make R large enough so that V can be ignored in the first term, and one can associate I_d with V_{app}/R at each FDTD time step, using as initial conditions the state of the PISCES simulation at the end of the previous time step. Thus, the boundary condition (5) becomes equivalent to (4).

We have tested this procedure on a case with known behavior—namely a diode at the end of a transmission line, as depicted in Fig. 1(b). The time scale for the electromagnetic signal was very long, so that we were assured to have steady state device behavior by the end of each FDTD time step.

To perform this test, first we employed the analytic I-V formula for an ideal diode, i.e.,

$$I(V) = I_s(e^{V/V_0} - 1) \tag{6}$$

for which I_s is the saturation current, $V_0 = q/\kappa T$ with q the electron charge, κ Boltzmann's constant and T the electron temperature. We placed this in (4) and integrated analytically over an FDTD time step $\Delta t = t^{(m+1)} - t^{(m)}$, with $u = e^{V/V_0}$, and $a = 1 + I_d/I_s$ to produce

$$\frac{CV_0}{I_d}\left[\log\left(\frac{u}{u-a}\right)\Big|_{V^{(m)}}^{V^{(m+1)}}\right] = \Delta t \tag{7}$$

yielding $E_y^{(m+1)} = V^{(m+1)}/\Delta y$ at the location of the diode for the next FDTD update (1b). A 10 volt sinusoidal signal was applied at

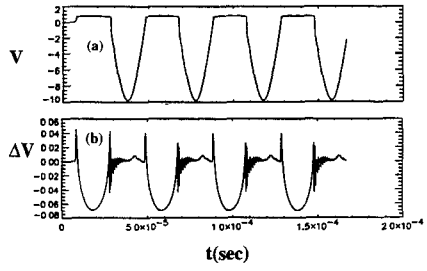

Fig. 2. (a) Time dependent voltage across a diode at the end of a transmission line. Solid: Ideal analytically integrated voltage. Dashed: PISCES integrated voltage, including external displacement current effects. (b) Deviation: $V_{PISCES} - V_{ideal} = \nabla V$.

the end of the line, and evaluated for 150 μsec. The solid line in Fig. 2(a) shows the resultant voltage across the diode. The signal is properly clipped at positive voltages when the diode is conducting.

Next, we used (5), and our abrupt-start trick to calculate $V^{(m+1)}$ and $E_y^{(m+1)}$ from PISCES. We plot the resultant diode voltage for the same sinusoidal input as the dashed curve in Fig. 2(a). Fig. 2(b) shows that the deviation from ideal is small, validating the new approach. The PISCES approach is, of course, much more general, and can be used with higher frequency input to calculate the net transient response of the coupled transmission line and device.

III. Conclusion

We have shown how a direct integration approach for simple lumped elements can improve the numerical properties of models employing FDTD analysis. More significantly, we have developed a noninvasive procedure by which standard PISCES-like software can be combined with FDTD to model the coupled internal dynamics of devices with external electromagnetics.

Acknowledgment

The authors would like to thank E. Harrigan of CRI.

References

[1] A. Taflove, "Basis and application of finite-difference time domain (FDTD) techniques for modeling electromagnetic wave interactions, short course notes," in *1992 IEEE Antennas Propagat. Soc. Int. Symp. and URSI 21 Radio Sci. Meet.*, July 1992, Chicago, IL.

[2] W. Sui, D. A. Christiansen, and C. H. Durney, "Extending the two-dimensional FD-TD method to hybrid electromagnetic systems with active and passive lumped elements," *IEEE Trans. Microwave Theory Tech.*, vol. 40, pp. 724–730, Apr. 1992.

[3] V. A. Thomas, M. E. Jones, M. Piket-May, A. Taflove, and E. Harrigan, "The use of SPICE lumped circuits as sub-grid models for FDTD high speed electronic circuit design," *IEEE Microwave and Guided Wave Lett.*, vol. 4, no. 5, pp. 141–143, May 1994.

[4] L. W. Nagel, "SPICE2: A computer program to simulate semiconductor circuits," University of CA, Berkeley, Rep. No. M520, May 1970.

[5] M. R. Pinto, C. S. Rafferty, and R. W. Dutton, "PISCES-II: Poisson and continuity equation solver," Stanford Electronics Lab. Tech. Rep., Sept. 1984.

[6] K. S. Yee, "Numerical solution of initial boundary value problems involving Maxwell's equations in isotropic media," *IEEE Trans. Antennas Propagat.*, vol. 14, no. 5, pp. 302–307, 1966.

[7] R. Holland, L. Simpson, and K. S. Kunz, "Finite Difference Analysis of EMP Coupling to Lossy Dielectric Structures," *IEEE Trans. Electromagn. Compat.*, vol. 22, no. 2, p. 203, 1980.

[8] D. Scharfetter and H. Gummel, "Large signal analysis of a silicon read diode oscillator," *IEEE Trans. Electron Devices*, vol. ED-16, no. 1, pp. 66–77, Jan. 1969.

On the Time Step in Hybrid Symmetrical Condensed TLM Nodes

Vladica Trenkic, Christos Christopoulos, and Trevor M. Benson

***Abstract*— New formulas for the maximum permissible time step in TLM hybrid nodes modeling anisotropic media are introduced and analyzed. It is shown that the value of the time step in most cases can be higher than that suggested by the minimum node dimension. The chosen value of the time step has significant impact on the dispersion characteristics of the hybrid symmetrical condensed node.**

I. Introduction

The hybrid symmetrical condensed node (HSCN) for the TLM method was originally described in [1]. Further generalizations of this node and a complementary HSCN were recently proposed in [2]. In the original HSCN [1], referred to as Type I in [2], all required inductances are modeled in the transmission lines, while open-circuit stubs are used to make up for any deficit in capacitances. A complementary Type II HSCN introduced in [2] models extra capacitances by altering the characteristic impedances of transmission-lines and uses short-circuit stubs to make up for any deficit in inductances.

The HSCN can operate with a larger time step than the stubbed SCN [3] due to the fact that the time step is not strictly dependent on the ratio of the largest to the smallest node dimension. Some considerations and comparisons of the maximum time step in the HSCN modeling isotropic media are given in [4], [5]. In the formulation of the HSCN for anisotropic media [2], the time step was related to the smallest mesh dimension Δl as $\Delta t = \Delta l/(2c)$. However, the maximum permissible time step was not defined.

In this paper we introduce the complete formulation for the maximum time step allowed in the HSCN for modeling anisotropic materials, based on the condition that characteristic admittances of the stubs must be nonnegative when modeling a passive medium [6]. We show that in most cases the value of the time step can be higher than that stated in [2]. Moreover, we demonstrate that dispersion characteristics of the HSCN are dependent on the chosen time step.

II. Maximum Time Step for HSCN

Contrary to the derivations in [1] and [2] where normalized characteristic admittances of stubs are given in terms of the smallest node dimension Δl, derivations in [5] are given directly in terms of the time step Δt. For an isotropic medium with electrical parameters ε_r, μ_r and a node with dimensions Δx, Δy, Δz, the normalized stub characteristic admittances for the Type I HSCN are given as [5]

Manuscript received November 28, 1994; revised May 25, 1995. This work was partially supported by EPSRC, UK.

The authors are with the Department of Electrical and Electronic Engineering, University of Nottingham, NG7 2RD Nottingham, UK.

IEEE Log Number 9413412.